

# Statistics of relativistically broadened Fe $K_\alpha$ lines in AGN

Matteo Guainazzi<sup>1,\*</sup>, Stefano Bianchi<sup>1</sup>, Michal Dovčiak<sup>2</sup>

<sup>1</sup> European Space Astronomy Centre of ESA, Apartado 50727, E-28080 Madrid, Spain

<sup>2</sup> Astronomical Institute, Academy of Sciences of the Czech Republic, Boční II 1401, 14131 Prague, Czech Republic

Received 30 August 2006

**Key words** quasars: emission lines – galaxies: nuclei – galaxies: active – X-ray: galaxies – line: profiles

We present preliminary results on the properties of relativistically broadened Fe  $K_\alpha$  lines in a collection of more than 100 Active Galactic Nuclei (AGN) observed by the XMM-Newton EPIC-pn camera. Our main conclusions can be summarized as follows: a) we detect broad lines in about 25% of the sample objects. This fraction increases to  $42 \pm 13\%$  if we consider only objects with more than  $10^4$  counts in the hard (2–10 keV) band, and to  $50 \pm 32\%$  for the small sub-sample (6 objects) of type 1 Piccinotti AGN with optimal XMM-Newton exposure (at least  $2 \times 10^5$  counts in the hard band); b) we find no significant difference in the detection rate of broad lines between obscured and unobscured AGN; c) the strongest relativistic profiles are measured in low-luminosity ( $L_X < 10^{43}$  erg s<sup>-1</sup>) AGN; d) Equivalent Widths (EWs) associated with relativistic profiles in stacked spectra are  $\lesssim 150$  eV for all luminosity classes; e) models of relativistically broadened iron line profiles (kyrline, Dovčiak et al. 2005), which include full relativistic treatment of the accretion disk emission around a Kerr black hole in the strong gravity regime, yield an average disk inclination angle  $\simeq 30^\circ$ , and a radial dependence of the disk emissivity profile  $\simeq -3$ . The distribution of EW is very broad, with  $\langle \log(EW) \rangle = 2.4$  and  $\sigma_{\log(EW)} = 1.4$ . We estimate that an investment of about 1 Ms of XMM-Newton time would be required to put these results on a sound statistical basis.

© 2006 WILEY-VCH Verlag GmbH & Co. KGaA, Weinheim

## 1 Introduction

XMM-Newton is the most suitable mission to study the properties of broad iron  $K_\alpha$  emission lines, thanks to the unprecedented collecting area of its EPIC cameras. As this workshop has demonstrated, the observational properties of the Fe emission line complex have been one of the primary subjects of AGN studies with XMM-Newton (see Fabian, this volume, and references therein). Although most of the papers in this field have focused on the detailed properties of the iron line profile in individual bright AGN, there have appeared in the literature some attempts to estimate the statistical importance of relativistic effects. Stacking spectra of a large sample of  $z \sim 1$  AGN in the Lockman Hole, for instance, Streblyanska et al. (2005) unveiled a relativistically broadened and skewed profile in both type 1 and type 2 objects. The Equivalent Width, EW, of such a feature is large (in the range 420–560 eV for unobscured, 280–460 eV for obscured AGN, depending on the profile models used). However, broadened iron  $K_\alpha$  lines with such a large EW are uncommon in the local universe (cf., e.g., the distribution of the broad Fe line EWs in a sample of 40 PG quasars studied by Jiménez-Bailón et al. 2005 in Fig. 1).

After almost seven years of successful XMM-Newton operations, it's time to give a systematic look backward at the wealth of data contained in the archive. This is the ap-

proach that has inspired the study presented in this paper. We aim at answering primarily the following questions:

- how often are effects due to X-ray illumination of a relativistic accretion disk detected in AGN?
- what do the properties of relativistically broadened profiles tell us about the accretion flow in the innermost regions around super-massive black holes?

### 1.1 The sample

The sample comprises 102 AGN observed as pointed nominal targets by XMM-Newton, and whose data were available in the public archive as of June 2006. Out of them: 32 are classified as Seyfert 1s, 18 as Narrow Line Seyfert 1s (NLSy1s), 39 are Radio Quiet Quasars (RQQs), and 13 are Seyfert 2s. No attempt has been made to create a complete and unbiased sample. We have restricted our study to Compton-thin obscured Seyfert 2s, whose nuclear emission is covered by a column density  $N_H \leq 10^{22.5}$  cm<sup>-2</sup>, because the determination of the  $K_\alpha$  iron line profile in spectra affected by stronger obscuration is uncertain. Most of the objects are local, with  $\simeq 60\%$  of them having a redshift  $< 0.1$ , and 98% of them  $< 0.5$ .

## 2 Data reduction and analysis

For each of the observations, data have been reduced from the *Observation Data Files* using SASv6.5 (Gabriel et al.

\* Corresponding author: Matteo Guainazzi. e-mail: Matteo.Guainazzi@sciops.esa.int

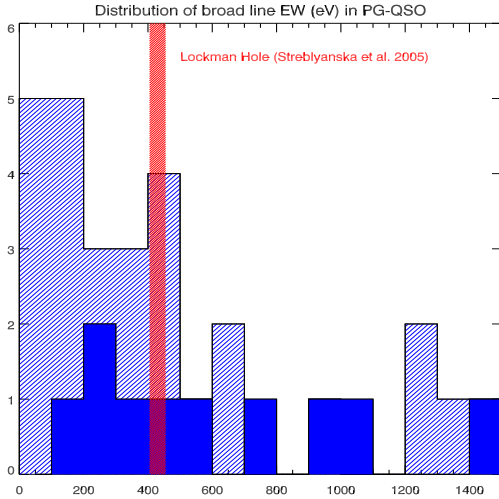


**Fig. 1** Distribution of the Fe  $K_{\alpha}$  line broad component EW in the sample of 40 PG quasars studied by Jiménez-Bailón et al. (2005). *Shaded cells* represent 90% confidence level upper limits. The measured EW in Lockman Hole unobscured AGN [after Tab. 1 in Streblyanska et al. (2005)] is marked by the *hatched rectangle* [ $420 \pm 35$  eV when the broad line is modeled with a Gaussian profile, as in Jiménez-Bailón et al. (2005)].

2003), and the most advanced calibration files available as of March 2006. We present in this paper data from the pn camera (Strüder et al. 2001) only, given its larger effective area. Spectra were extracted using standard pattern event selection. The radius of the circular spectral extraction regions and the count rate background rejection thresholds were chosen in order to maximize the signal-to-noise in each individual spectrum. Background spectra were extracted from nearby circular areas in the same chip as the source, except for observations in Small Window mode, where blank field event list (Read & Ponman 2003) were used, after coordinate recasting and normalization to the quiescent background level. For the time being, we have not merged different observations of the same target. Whenever multiple observations are available, we have used that with the longest “good” exposure time (except in Fig. 2, see Sect. 3).

All the spectra have been rebinned, in order to ensure that each background-subtracted spectral channel has at least 25 counts, and that the instrumental energy resolution is not oversampled by a factor larger than 3. Spectra have been fit in the 2.5–15 keV energy range. We have employed the following baseline fitting model:

$$e^{-\sigma_{ph} N_H} \times A [E^{-\Gamma} + C(\Gamma, \phi, E) + \sum_{i=1}^3 G_i + B(\phi, \beta, a)] (1)$$

where  $\sigma_{ph}$  is the photoelectric cross-section (Anders & Grevesse 1989),  $N_H$  is the column density (constrained not to be lower than the contribution due to intervening gas in our Galaxy),  $C$  is a Compton-reflection component by a plane-parallel neutral slab (model `pexrav` in XSPEC; Magdziarz & Zdziarski 1995),  $G_i$  are Gaussian unresolved profiles with

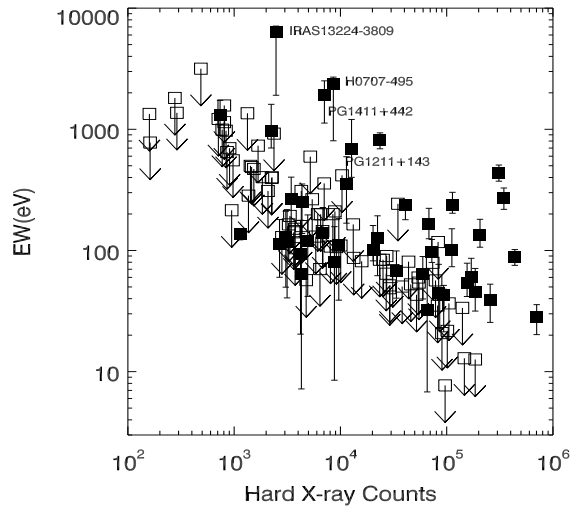


**Fig. 2** EW of the relativistically broadened Fe  $K_{\alpha}$  line against the net hard (*i.e.* 2–10 keV) counts. Each data point corresponds to one XMM-Newton observation. Multiple observations of the same objects are shown as distinct points. *Filled squares* represent line detections, *empty squares* represent upper limits. Source excluded from the sample are labeled (see text for details). The three objects with EW upper limits  $< 20$  eV are: IC4329A (see, *e.g.* Gondoin et al. 2001, Steenbrugge et al. 2005), Mkn 509 (Pounds et al. 2001), NGC7469 (Blustin et al. 2003).

centroid energy 6.4 keV (FeI), 6.7 keV (FeXXV), and 6.96 keV (FeXXVI), and  $B$  is a relativistically broadened profile. We have used for  $B$  model profiles as predicted around Schwarzschild ( $a = 0$ ; Fabian et al. 1989) and Kerr ( $a \simeq 1$ ; Laor 1991) black holes, as well a set of models (`kyrline`; Dovčiak et al. 2005), which includes full relativistic treatment of the accretion disk emission around a Kerr black hole in the strong gravity regime. The `ky` model family depends on the disk inclination angle  $\phi$ , on the radial dependence of the emissivity (power-law index  $\beta$ ) and on the dimensionless black hole spin  $a$ . In order not to over-fit the data in moderate statistical quality spectra, we have employed the  $\beta$  parameter only as a measurement of the strength of relativistic effects, while fixing the innermost and outermost radii of the line-emitting region to the innermost stable circular orbit for a given  $a$  value, and to 400 gravitational radii, respectively.

### 3 Detection of relativistic lines in individual spectra

In Fig. 2 we show the EW of the Fe  $K_{\alpha}$  relativistically broadened component as a function of the total net counts in the 2–10 keV band. As expected, the overwhelming majority of the measurements are aligned along a straight line (in log-log space), which represents the sensitivity limit of our sample. Three poorly exposed ( $< 10\,000$  hard counts)

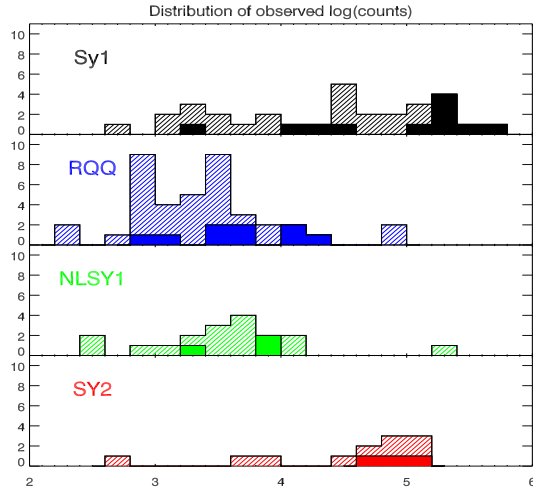


**Fig. 3** Distribution of the net counts in the hard X-ray band for the AGN of our sample. *Filled cells* correspond to detections of a broad iron  $K_{\alpha}$  profile; *shaded cells* to non-detections.

AGN type	Well exposed (%)	Underexposed (%)
Seyfert 1s	$50 \pm 15$	$< 21$
RQQs	$60 \pm 48$	$17 \pm 8$
NLSy1 s	$< 30$	$20 \pm 14$
Seyfert 2s	$33 \pm 24$	$< 30$

**Table 1** Fraction of broad iron  $K_{\alpha}$  detections in our AGN sample. Errors are at the  $1\sigma$  level

objects are well above this correlation, and exhibit EW by an order of magnitude larger than the average of the sample at their net count level. They are: IRAS 13224-3809, PG1411+442, and 1H 0707-495. In the last the presence of a  $EW > 1$  keV relativistically broadened Fe  $K_{\alpha}$  line has been challenged (Gallo et al. 2004, Fabian et al. 2004). We therefore consider these detections as “suspicious”, and removed these objects from the sample. For similar reason, we exclude from the sample PG1211+143 (Pounds et al. 2003). None of the sample results presented in this paper is significantly affected by this choice.

The distribution of the source counts is shown in Fig. 3. In these histograms, *filled cells* represent objects where a broad Fe  $K_{\alpha}$  iron line is detected, *shaded cells* represent non-detections (the distribution of the EW upper limits is shown in Fig. 4). The fraction of detections is  $42 \pm 13\%$  and  $16 \pm 6\%$  for “well-exposed”, and “under-exposed” objects, respectively, where we have arbitrarily set a threshold of 10000 net counts to distinguish the two classes. The detection fraction is not significantly dependent on the AGN type (Tab. 1); however, the small number statistics prevents strong statement from being drawn.

In Fig. 5 normalized distribution functions are shown for the best-fit parameters on which the *kyrline* model

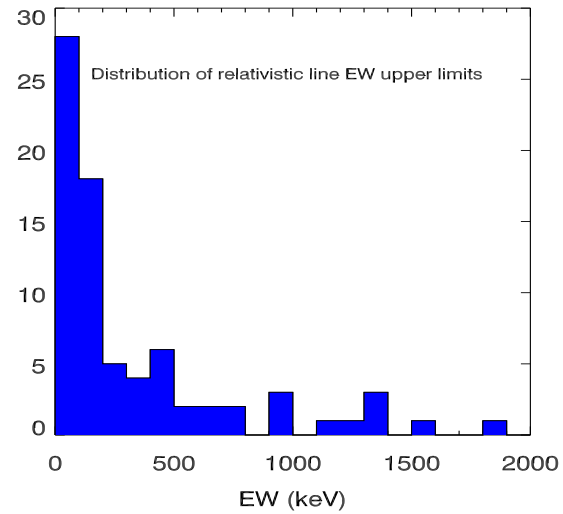


**Fig. 4** Distribution of upper limits on the EW of the broad iron  $K_{\alpha}$  line in our sample.

Parameter	$\langle \rangle$	$\sigma$	$N_{obj}$
$\beta$	-2.6	1.8	22
$\phi$	33	21	21
$\log(EW)$	2.4	1.4	20

**Table 2** Mean and standard deviations on  $\beta$ ,  $\phi$ , and  $EW$  in our sample.  $N_{obj}$  is the number of objects on which a statistically meaningful constraints on the parameter can be set, and which have been used to construct the normalized distributions in Fig. 5

depends. These distributions are generated combining one Gaussian distribution for each individual measurement, whose mean (standard deviation) is the best-fit value (statistical error). In Tab. 2 the mean ( $\langle \rangle$ ) and standard deviation ( $\sigma$ ) of the combined distributions are listed, together with the number of measurements used to construct the normalized distribution. In 5 objects a constraints on the black hole spin can be derived ( $\langle a \rangle = 0.6$ ,  $\sigma_a = 0.3$ ). In two of them (HE1029-1401,  $a = 0.85 \pm 0.04$ ; NGC 3227,  $a < 0.18$ ) the measurement is formally inconsistent with a maximally spinning black hole; in the other three (MCG-6-30-15, NGC 3516, NGC 4395) only a lower limit on  $a$  can be derived.

Several authors have discussed the effect that the spectral curvature produced by high-density ionized absorbers may have on the detectability of broad Fe  $K_{\alpha}$  profiles (Reeves et al. 2004, Pounds et al. 2003, Turner et al. 2005; see as well Diaz-Trigo’s and Reeves’ papers in this volume). If not properly accounted for by “warm absorbers” models, this curvature may mimic the red wings of a relativistic broadened profile in the 3–6 keV energy range. Approximating an ionized absorber with a cold absorber - as done with model (1) - might be too crude.

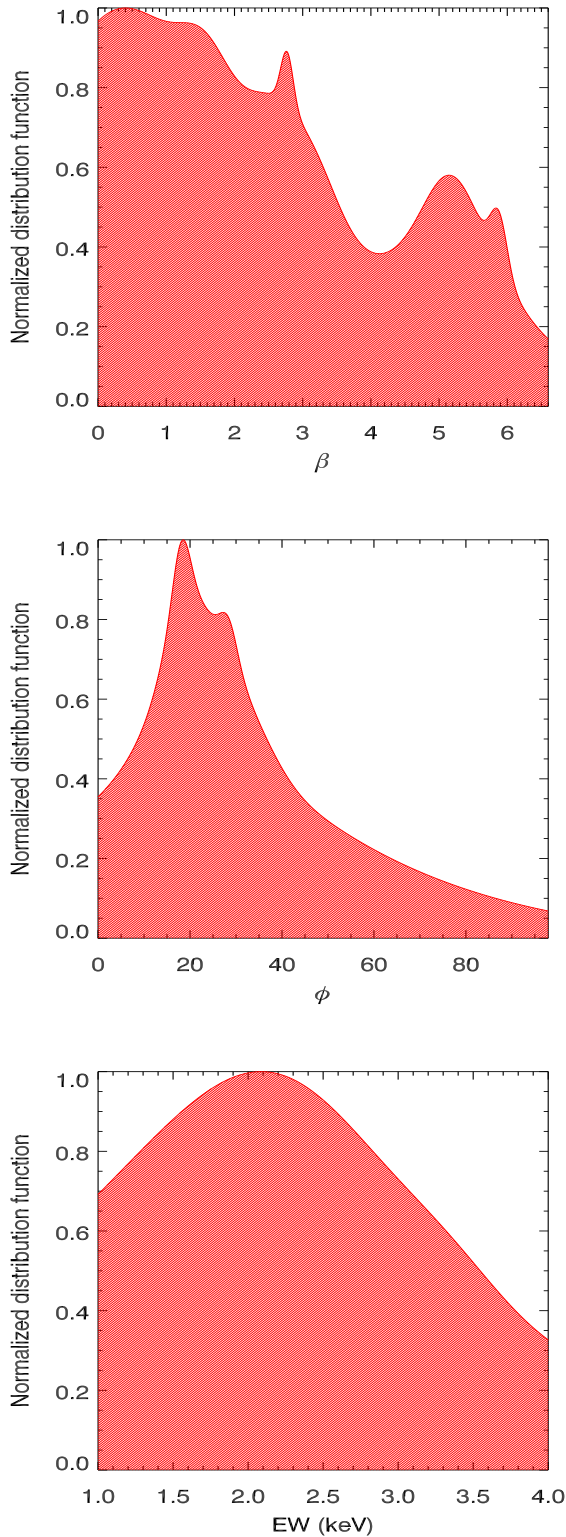


**Fig. 5** Normalized distribution functions for  $\beta$ ,  $\phi$  and EW.

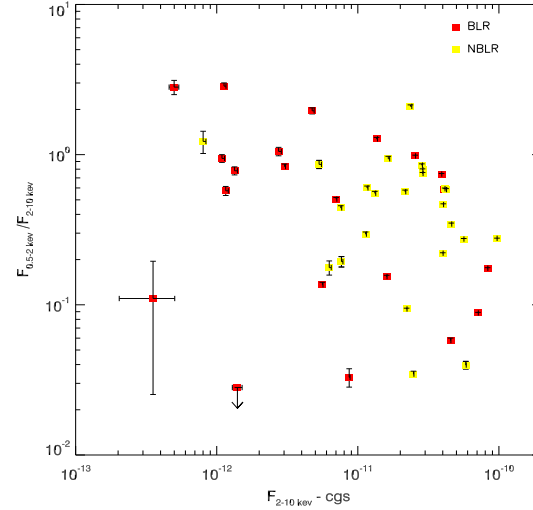


**Fig. 6** Softness flux ratio against 2–10 keV flux for the AGN of our sample, where only an upper limit on the EW of the iron  $K_{\alpha}$  broad component is found (*red squares*) and AGN where a broad iron  $K_{\alpha}$  line is detected (*yellow squares*).

In Fig. 6 we plot the 0.5–2 keV versus 2–10 keV softness ratio for the objects of our sample, separating with different colors objects where only an upper limit on the broad Fe  $K_{\alpha}$  line  $\leq 100$  eV has been measured from objects where a broad line has been detected. The softness ratio should be sensitive to the presence of “warm absorbers”, which imprint strong absorption features in the soft band<sup>1</sup>. We find no difference in the softness ratio in the two classes. We conclude that it is unlikely that the number of iron  $K_{\alpha}$  broadened line detections is significantly affected by uncertainties in the underlying warm absorbed continuum determination (although in individual objects this effect may have an important impact, as discussed by the above referred authors).

#### 4 Detection of relativistically broadened profiles in stacked spectra

Relativistically broadened iron  $K_{\alpha}$  profiles have been detected in about 25% of the sources of our sample. In at least 50% of the sample, the upper limits on the EW of a relativistically broadened profile are inconclusive as to establishing whether such a feature is present (cf. Fig. 3 and 4).

This statistical limitation, however, can be overcome, by stacking data together. In Fig. 7 we show stacked residuals for the objects of our sample, once they have been divided in four, equally populated (as of number of sources) 2–10 keV absorption-corrected luminosity classes. The stacked residuals were generated by summing together the residuals of

<sup>1</sup> This ratio is actually mostly sensitive to standard warm absorbers with photoionization parameters  $\xi \sim 10\text{--}100$  and  $\log(N_H) \sim 21\text{--}22$   $\text{cm}^{-2}$  (Blustin et al. 2005). However, high-density, high-ionization warm absorber are often found in conjunction with lower-density, low ionization counterparts.

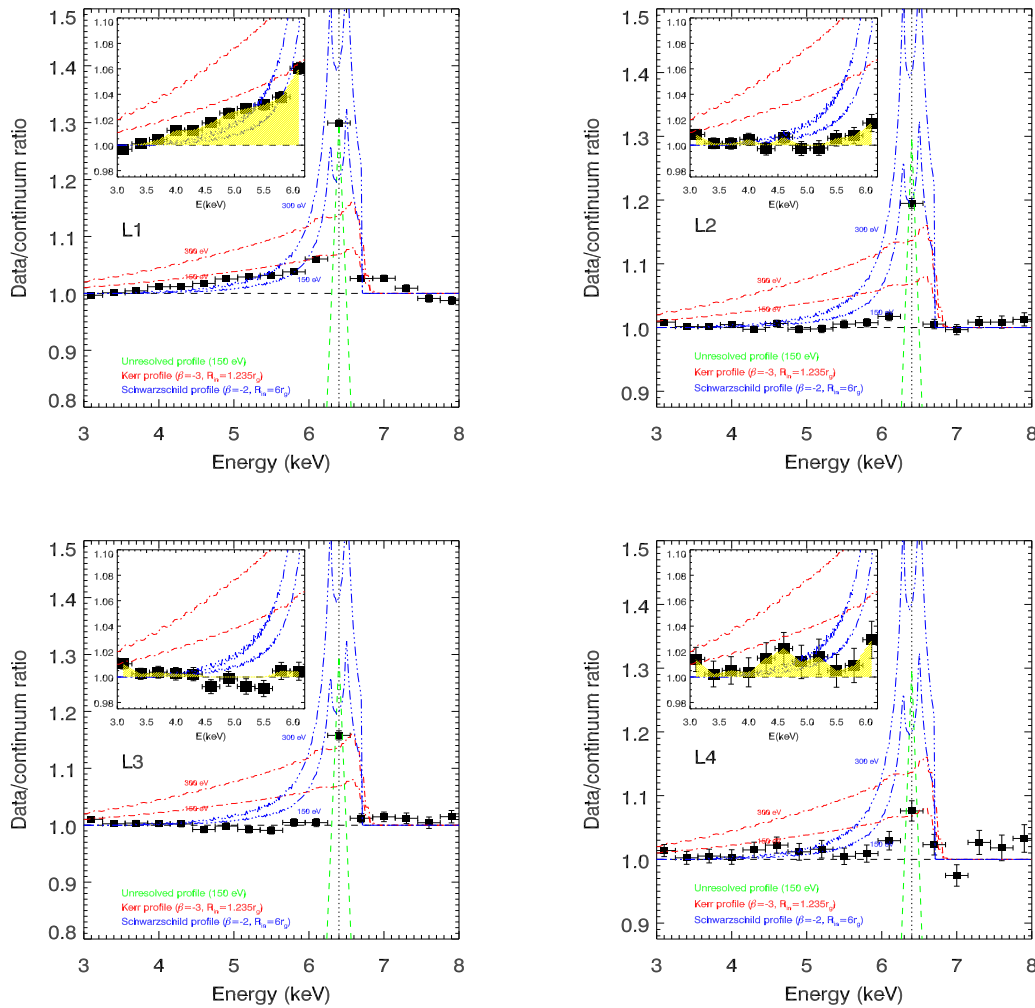


**Fig. 7** 3–8 keV (3–6 keV in the *insets*) stacked residuals for the AGN of our sample, divided in four equally-populated 2–10 keV intrinsic luminosity bins. The curves represent the: a) expected profile of an unresolved Gaussian profile, reflecting the intrinsic pn camera energy resolution (*dashed line*); b) two maximally rotating Kerr profiles corresponding to  $\text{EW}=150$  eV and 300 eV (*dot-dashed profiles*); c) two Schwarzschild profiles (*long dashed-dot line*) corresponding to the same values of EW. The luminosity bins are defined as follows: L1,  $L_X < 10^{43}$  erg s $^{-1}$ ; L2,  $10^{43} \leq L_X < 5 \times 10^{43}$  erg s $^{-1}$ ; L3,  $5 \times 10^{43} \leq L_X < 1.5 \times 10^{44}$  erg s $^{-1}$ ; L4,  $L_X \geq 1.5 \times 10^{44}$  erg s $^{-1}$

a fit with model (1), after the  $\sum_i G_i$  and  $B(\beta, \phi, a)$  terms had been removed. A clear broadened relativistic profile is present in the lowest luminosity sub-sample ( $L_X < 10^{43}$  erg s $^{-1}$ ) and possibly in the highest luminosity sub-sample. If the lowest luminosity bin is split into two equally-populated bins, the broad line keeps being stronger in the lower-luminosity bin (Fig. 8). It seems to exist a sort of “Baldwin effect” on the relativistically broadened component of the iron  $K_\alpha$ , similar to what already claimed on the narrow component of the same line (Iwasawa & Taniguchi 1993, Page et al. 2003; see as well Jiménez-Bailón et al. 2005 for a different interpretation of the same data).

Broadened profiles with comparable profiles are detected in the stacked residuals of luminosity-matched samples of Seyfert 1s and Seyfert 2s (see Fig. 9), although in the lat-

ter the profile is weaker. The integrated EW of the stacked profiles is  $\lesssim 150$  eV for any luminosity class (compare the observed profiles with the profiles of an extreme Kerr line in Fig. 7 to Fig. 9), therefore significantly lower than measured by Streblyanska et al. (2005) on the Lockman Hole AGN.

## 5 Can we achieve the full coverage of a complete sample?

The paradigm to explain the origin of the energy output in Active Galactic Nuclei (AGN) requires radiatively efficient accretion onto super-massive black holes (Lynden-Bell 1969). In this scenario, the accretion flow reaches the innermost regions close to the black hole, possibly the innermost circular stable orbit if it occurs in a standard geo-

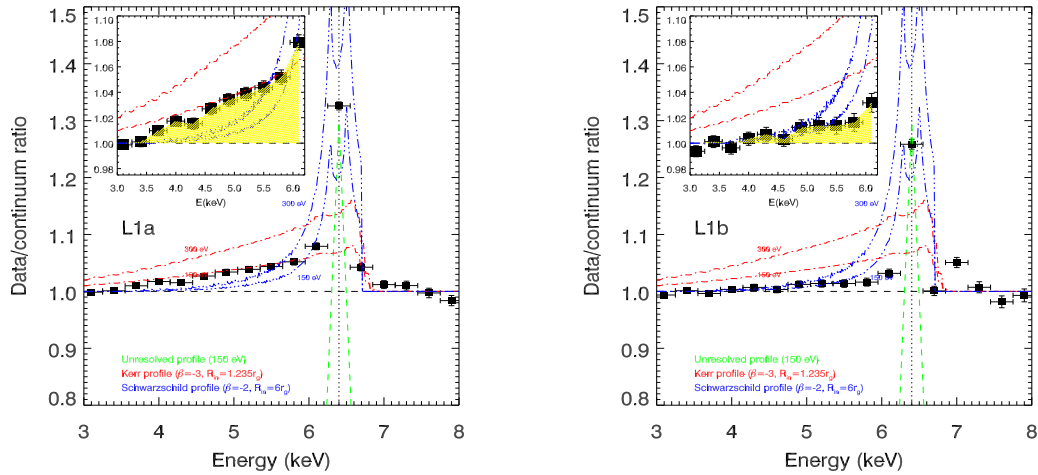


**Fig. 8** The same as Fig. 7, when the lowest-luminosity bin is split in two equally-populate (in source numbers) bins. The *left panel* corresponds to objects with  $L_X \leq 10^{42}$  erg  $s^{-1}$ , the *right panel* to  $10^{42} < L_X \leq 10^{43}$  erg  $s^{-1}$ .

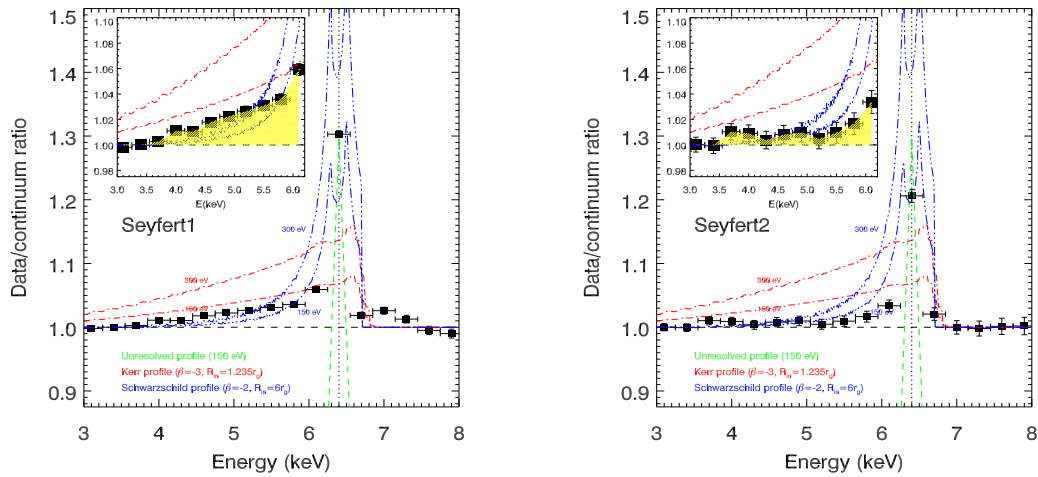


**Fig. 9** The same as Fig. 7, for luminosity-matched sub-samples of Seyfert 1s (*left panel*) and Seyfert 2s (*right panel*).

metrically thin and optically thick disk. An inescapable prediction of this scenario is that relativistic broadening and skewing of emission lines should be common in AGN. The measure of the “true” fraction of objects where relativistic effects are detected would be crucial to establish if and how the standard AGN paradigm needs to be modified. Current AGN samples in X-rays are inevitably biased towards bright AGN, and furthermore towards bright Seyferts where the detection of a relativistically broadened iron  $K_\alpha$  profile was expected on the basis of observations prior to the *Chandra* and XMM-Newton launches.

The AGN sample on which the study presented in this paper has been conducted is neither complete nor unbiased in any statistical sense. It is merely the collection of all the observations available in the XMM-Newton science archive at a given moment in time. This study needs to be extended (or restricted) to a statistically complete flux-limited sam-

ple before any inference can be derived on the true fraction of AGN where relativistic effects are important, as well as on the properties of the innermost regions of the accretion flow around super-massive black holes (or, hopefully, on the black hole spin itself). The double bias outlined above needs to be removed.

How can one build a complete sample, where the spectrum of each member of the sample has enough statistics for meaningful constraints on the properties of relativistically broadened iron  $K_\alpha$  lines to be derived? Let’s consider again the EW versus net counts correlation in Fig. 2. For counts  $\gtrsim 10^5$  the correlation flattens. This represents the minimum number of net counts necessary to detect a line as strong as the average of the EW distribution. Moreover, a number of net counts  $\gtrsim 2 \times 10^5$  ensures that a complete separation between measurements and upper limits is achieved. This condition is crucial to assess the significance of any non de-

tections. Hence, we conclude that in order to derive the true fraction of relativistic lines in a sample of AGN, each of the members of the sample has to be observed long enough to accumulate at least 200 000 net counts in the hard X-ray band.

If we take the Piccinotti sample (Piccinotti et al. 1982) as example of a flux-limited sample in the hard X-ray band, only 6 out of its 27 type 1 objects have been optimally exposed with XMM-Newton. The detection fraction of relativistically broadened iron  $K_{\alpha}$  lines in this sub-sample is  $50 \pm 32\%$ . We estimate that a full coverage of a hard X-rays flux limited sample such as the Piccinotti or the RXTE All Sky Survey (Revnivtsev et al. 2004) would require  $\sim 1$  Ms at a flux limit  $\simeq 2 \times 10^{-11}$  erg cm $^{-2}$  s $^{-1}$ . This is large but not unreasonable time allocation for an XMM-Newton Large Program.

## 6 Conclusions

The main conclusions of this study can be summarized as follows:

- relativistically broadened Fe  $K_{\alpha}$  lines are present in  $\simeq 50\%$  of well exposed XMM-Newton spectra
- the detection rate and average properties are not significantly different between type 1 and type 2 objects, although the analysis of stacked spectral residuals on luminosity well-matched samples of Seyfert 1s and Seyfert 2s suggests a possible weaker line in the latter
- the relativistically broadened Fe  $K_{\alpha}$  lines detected in our study cover a large range of EW. However, our stacked spectral residuals analysis finds typically  $EW \lesssim 150$  eV, far from the  $\simeq 500$  eV EWs claimed by Streblyanska et al. (2005) for the Lockman Hole AGN
- relativistically broadened Fe  $K_{\alpha}$  lines are significantly more common in low luminosity ( $L_X \leq 10^{43}$  erg s $^{-1}$ ) AGN
- the average disk inclination is  $\langle \phi \rangle = 34^\circ$ ; the average accretion flow power-law radial dependent index is  $\langle \beta \rangle = -2.7$
- in 4 out of 6 objects where the measurement of the dimensionless black hole spin yields meaningful constraints, the Schwarzschild solution can be ruled out

The conclusions of this study are still based on an incomplete and biased sample. However, a relatively modest investment of XMM-Newton time could allow them to be put on a firm statistical ground. **At least 200 000 hard X-ray counts are necessary to ensure an unambiguous detection, as well as a clear discrimination between detections and upper limits.** We estimate that around 1 Ms would be enough to optimally expose a hard X-ray flux limit sample at a flux limit  $\simeq 2 \times 10^{-11}$  erg cm $^{-2}$  s $^{-1}$ .

## References

Anders E. & Grevesse N., 1989, *Geochimica et Cosmochimica Acta* 53, 197

- Blustin A.J., Branduardi-Raymond G., Behar E., et al., 2003, *A&A*, 403, 481
- Blustin A.J., Page M.J., Fürst S.V., et al., 2005, *A&A*, 431, 111
- Dovčiak M., Karas V, Yaqoob T., 2005, *ApJS*, 153, 205
- Fabian A.C., Rees M.J., Stella L., White N.E., 1989, *MNRAS*, 238, 729
- Fabian A.C., Miniutti G., Gallo L., et al., 2004, *MNRAS*, 353, 1071
- Gabriel C., Denby M., Fyfe D. J., Hoar J., Ibarra A., 2003, in *ASP Conf. Ser.*, Vol. 314 *Astronomical Data Analysis Software and Systems XIII*, eds. F. Ochsenbein, M. Allen, & D. Egret (San Francisco: ASP), 759
- Gallo L.C., Tanaka Y., Boller Th., et al., 2004, *MNRAS*, 353, 1064
- Gondoin P., Barr P., Lumb D., et al., 2001, *A&A*, 378, 806
- Iwasawa K., Taniguchi Y., 1993, *ApJ*, 413, L151
- Laor A., 1991, *ApJ*, 376, 90
- Lynden-Bell D., 1969, *Nat*, 223, 690
- Jiménez-Bailón E., Piconcelli E., Guainazzi M., Scahrtel N., Rodríguez-Pascual P, Santos-LLeo M., 2005, *A&A*, 435, 449
- Magdziarz P. & Zdziarski A.A., 1995, *MNRAS* 273, 837
- Page K.L., O'Brian, Reeves J.N., Breeveld A.A., 2003, *MNRAS*, 340, 1052
- Piccinotti G., Mushotzky R.F., Boldt E.A., et al., 1982, *ApJ* 253, 485
- Pounds K., Reeves J., O'Brien P., et al., 2001, *ApJ*, 559, 181
- Pounds K., Reeves J.N., King A.R., et al., 2003, *MNRAS*, 345, 705
- Read A.M., Ponman T.J., 2003, *A&A*, 409, 395
- Reeves J.N., Nandra K., George I.M., et al., 2004, *ApJ*, 602, 648
- Revnivtsev M., Sazonov S., Yahoda K., Gilfanov M., 2004, *A&A*, 418, 927
- Steenbrugge K., Kaastra J.S., Sako M., et al., 2005, *A&A*, 432, 453
- Streblyanska A., Hasinger G., Finoguenov A., Barcons X., Mateos S., Fabian A.C., 2005, *A&A*, 432, 395
- Strüder L., Briel U., Dannerl K., et al., 2001, *A&A* 365, L18
- Turner T.J., Kraemer S.B., George I.M., Reeves J.M., Bottorff M.C., 2005, *ApJ*, 618, 155